CrossMark

How Meteor Showers Can Guide the Search for Long-period Comets

Samantha Hemmelgarn[1,2] , Nicholas Moskovitz[1] , Stuart Pilorz[3], and Peter Jenniskens[3]
[1] Lowell Observatory, 1400 West Mars Hill Road, Flagstaff, AZ 86001, USA; shemmelgarn@lowell.edu
[2] Department of Astronomy and Planetary Science, Northern Arizona University, P.O. Box 6010, Flagstaff, AZ 86001, USA
[3] SETI Institute, 339 Bernardo Ave., Mountain View, CA 94043, USA

Abstract

With orbital periods longer than 200 yr, most long-period comets (LPCs) remain undiscovered until they are inbound toward perihelion. The comets that pass close to Earth's orbit are potentially hazardous objects. Those with orbital periods up to $\sim$4000 yr tend to have passed close to Earth's orbit in a previous orbit and produced a meteoroid stream dense enough to be detected at Earth as a meteor shower. In anticipation of Rubin Observatory's Legacy Survey of Space and Time (LSST), we investigate how these meteor showers can guide dedicated searches for their parent comets. Assuming search parameters informed by LSST, we calculated where the 17 known parent bodies of LPC meteor showers would have been discovered based on a cloud of synthetic comets generated from the shower properties as measured at Earth. We find that the synthetic comets predict the on-sky location of the parent comets at the time of their discovery. The parent comet's location on average would have been $1°.51 \pm 1°.19$ from a line fit through the synthetic comet cloud. The difference between the heliocentric distance of the parent and mean heliocentric distance of synthetic comets on the line was 2.09 ± 1.89 au for comets with unknown absolute nuclear magnitudes and 0.96 ± 0.80 au for comets with known absolute nuclear magnitudes. We applied this method to the σ-Hydrids, the proposed meteor shower of comet Nishimura, and found that it successfully matched the pre-covery location of this comet 8 months prior to Nishimura's discovery.

1. Introduction

Meteor showers are caused by streams of meteoroids that move in orbits similar to that of their parent comet. As comets approach perihelion, heat from the Sun warms their surface (K. J. Meech & J. Svoren 2004). Sublimation of gases drags solid particles (the meteoroids) off the nucleus and ejects them into independent orbits, similar to that of the comet because ejection speeds are much smaller than the velocity of the comet around the Sun (K. J. Meech & J. Svoren 2004; P. Jenniskens 2006; D. Tomko & L. Neslusan 2019). The meteoroids will follow slightly different trajectories based on their ejection velocity and the individual grain properties that affect the influence of solar radiation pressure (e.g., size, density, albedo). In returning at different times, these meteoroids disperse along the comet orbit, creating a stream. Over time, this dispersion will typically increase due to gravitational and nongravitational perturbations (P. Jenniskens 2006; Q. Ye 2016).

Meteor showers sample a subset of all meteoroids in the stream, i.e., only those that intersect Earth's orbit and impact Earth. Earth's intersection with meteoroid streams produces the meteor showers we see in the night sky. A streak of light occurs as meteoric matter is heated and ablated high up in the atmosphere. From that streak, the meteoroid speed and direction of motion can be measured to determine the pre-impact orbit in space.

The population of long-period comets (LPCs) includes a group that have detectable meteoroid streams: a trail of breadcrumbs that indicate the comet's presence. LPCs have orbital periods larger than 200 yr, too long to resonate with the motion of the planets. Those comets that have orbital periods (P) shorter than about 4000 yr are known to produce detectable meteor showers at Earth (P. Jenniskens et al. 2021). Comets in longer orbits will produce meteoroid streams that become too diluted to be detected as meteors on Earth.

In recent years, large networks of low-light video camera arrays have been built to map the orbits of LPC meteoroid streams. Observations with the Cameras for All-sky Meteor Surveillance (CAMS) network were initiated in 2010, and since then, these camera networks have constrained roughly 3 million meteor orbits (P. Jenniskens et al. 2011; D. Zubović et al. 2015). The IAU currently recognizes 110 confirmed meteor showers and another 823 awaiting confirmation. A total of 513 showers are described in P. Jenniskens (2023), half of which are caused by LPCs. Only 17 of these have known or suspected parent bodies.

A search strategy to find LPCs based on observed meteor shower orbits at Earth was put forth in P. Jenniskens et al. (2020). There the authors used a detected outburst of the 15-Bootids detected by CAMS to constrain a search region on sky for the parent comet by projecting the median Keplerian orbital elements of the outburst to potential positions of the parent comet onto the sky. This approach can help find LPCs earlier than in routine searches, which would provide extra warning time before an imminent impact.

Potentially hazardous objects (PHOs) are those comet or asteroid near-Earth objects (NEOs) that pose an impact hazard to Earth. PHOs have absolute magnitudes (H) < 22 and a minimum orbit intersection distance < 0.05 au. In 1998, NASA set out to catalog all NEOs with a diameter larger than 1 km. Within 13 yr, 90% of the NEOs on short orbits had been discovered and cataloged (A. Mainzer et al. 2011). Not yet discovered are many of the NEO LPCs, which return to the inner solar system infrequently. The rate of impacts from LPCs

could be up to 6% of all impacts on Earth (S. N. Quintana & P. H. Schultz 2019).

The destructive nature of a single LPC impact is strong motivation to be proactive about the hazards posed by them. Most comets are $\geqslant 1$ km in diameter. The impact of an LPC as small as 1 km can have global consequences because of their high impact velocities. Cometary impact velocities can be as high as $72 \, \text{km s}^{-1}$ and are typically $\sim 50 \, \text{km s}^{-1}$ (B. Marsden & D. Steel 1994; P. R. Weissman 2007; J. A. Nuth et al. 2018). A 1 km comet of average density, $0.6 \, \text{g cm}^{-3}$ (P. R. Weissman 2007; J. A. Nuth et al. 2018), traveling at $50 \, \text{km s}^{-1}$ would impact Earth with roughly the energy of 750,000 megatons of TNT. An impact of this scale could lead to global cooling and ozone layer loss (O. B. Toon et al. 1994).

The probability of such an impact on any given perihelion passage remains low, on the order of 1×10^{-9} (B. Marsden & D. Steel 1994) for the whole population. However, among the total population of Oort Cloud comets $\geqslant 1$ km with perihelion distances less than 5 au estimated to be in the range of 1×10^{12} objects (B. Boe et al. 2019), there are ~ 1000 LPCs that could strike Earth on their next perihelion passage. Of these, ~ 200 have orbital periods small enough to have detectable meteoroid streams.

At present, defending against a potential LPC impactor is made difficult due to the relatively short warning time between discovery and impact (D. Morrison 2006; J. A. Nuth et al. 2018). LPCs are typically discovered around 5 au from the Sun, which only provides up to 2 yr warning time to mitigate the impact risk (C. Gritzner et al. 2006). In the near future, new technologies will push that detection limit, with the wide-field Legacy Survey of Space and Time (LSST) expecting to see first light in 2025. The potential to discover these comets farther out in the solar system will become greater, providing more warning time in the case of a potential impactor.

If meteor showers could guide the search for LPCs, then dedicated searches could take advantage of these technologies to discover them. The LSST, for example, proposes to take 1000 images of the same patch of sky in a 10 yr period (LSST Science Collaboration et al. 2009) and will have the ability to see objects up to a limiting magnitude of 24.5 per exposure (Z. Ivezić et al. 2019). This limit could be pushed several magnitudes fainter with image stacks that take into account the known rate of motion of the comet.

Here we explore the method of P. Jenniskens et al. (2020) further to investigate how much warning time is gained by using meteoroid streams to guide dedicated deep searches for approaching LPCs and how feasible such searches are.

2. Methods

To investigate the use of meteor shower data in guiding searches for their LPC parents, we investigated how the 17 known LPC parent bodies (Table 1) would have been detected in a dedicated search.

Note that not all comet shower associations are certain. Parent body associations to meteor showers are typically determined by comparing median orbits by a method known as the D-criterion of R. B. Southworth & G. S. Hawkins (1963). This criterion calculates how dissimilar two orbits are. J. D. Drummond (1981), T. J. Jopek (1993), G. B. Valsecchi et al. (1999), P. Jenniskens (2008), T. J. Jopek et al. (2008), A. Rożek et al. (2011), and R. Rudawska et al. (2015) have all expanded on R. B. Southworth & G. S. Hawkins (1963) to

provide additional methods for determining parent/shower association. However, dynamical modeling of debris ejected from the shower's potential parent is a better method to confirm these associations (e.g., D. Šegon et al. 2017). Here we refer to those past studies, summarized in P. Jenniskens (2023), and evaluate the likelihood of the proposed associations from our analysis.

2.1. Range of Possible Comet Positions on Sky

For each case, we created a cloud of synthetic comets based solely on the observed dispersion of the meteor shower orbital elements measured at Earth (Table 1). A "search region," for the purposes of this analysis, is defined as the solid angle subtended by the cloud of synthetic comets. We defined a heliocentric distance (r) range that would put the synthetic comets just beyond current survey brightness limits ($V \sim 22$), yet consistent with expected LSST capabilities ($V < 25$), and calculated where the known comet would have been detected relative to the cloud had LSST been operating. We fit a line through the cloud of synthetic comets to conduct our analysis. We then determined how far from the center of the cloud the comet would have been located, how far it would have been from Earth's orbit, and how much extra warning time would have been provided.

We used the nominal H and its corresponding heliocentric distance range for six comets with known H values. For those that did not have known H values, we kept this as a free parameter and defined the suitable range of r for each integer absolute magnitude between $10 \leqslant H \leqslant 17$ (Figure 1).

We then determined in which part of the orbit the comet approached perihelion and was within heliocentric distances corresponding to visual magnitudes (V) between $22 \leqslant V \leqslant 25$. For example, a comet with an $H = 14$ would have $6.224 \leqslant r \leqslant 11.887$ where V was within this specific range. Based on the time of perihelion, we determined the date on which our $H = 14$ parent comet was at $r = 6.224$, $r = 7$, $r = 8$, etc., up to $r = 11.887$. For each date (i.e., heliocentric distance), we created an ephemeris and projected onto the sky only the synthetic comets that were on LPC-like orbits ($200 \leqslant P \leqslant 4000$) and within our observability constraints, along with the position of the parent comet on that date. In all, we completed 850 simulations by following this process across 17 meteor showers.

2.2. Software Tools

Our calculation of projected comet positions on sky used the Python programming language and the open-source orbit computation program OpenOrb (M. Granvik et al. 2009). We used OpenOrb to calculate projected sky positions (R.A., decl.) on a given date (and thus position of Earth in its orbit) for an array of synthetic comets, derived from a uniform sampling of each meteoroid stream's measured dispersions. OpenOrb has functions that include orbit determination, mass determination, ephemeris generation, and orbit propagation. Ephemeris generation was the sole function that we used. The function reads an orbit file (which must be of file extension .orb or .des, with .des used here) containing orbital elements, absolute magnitude, date, and coordinate type (CAR: Cartesian; KEP: Keplerian; COT: cometary true anomaly; etc.). The IAU observatory code is a parameter that is specified during ephemeris generation to define the topocentric coordinates for

Table 1
Orbital Elements of the 17 Meteor Showers with Known LPC Parent Bodies

Shower/Parent	q (au)	e	i (deg)	ω (deg)	Ω (deg)
#6	0.921 ± 0.016	0.954 ± 0.162	79.5 ± 2.5	214.1 ± 4.3	32.3 ± 1.2
C/1861 G1	0.921	0.983	79.8	213.4	31.9
#23	0.784 ± 0.058	0.953 ± 0.166	170.8 ± 1.9	235.8 ± 9.9	205.2 ± 7.4
C/1987 B1*	0.870	0.996	172.2	200.4	176.0
#145	1.000 ± 0.005	0.953 ± 0.124	74.4 ± 2.2	191.3 ± 3.5	50.0 ± 1.6
C/1983 H1	0.991	0.990	73.25	192.9	49.10
#175	0.557 ± 0.056	0.964 ± 0.102	149.1 ± 1.8	265.6 ± 8.3	113.3 ± 10.6
C/1979 Y1	0.545	0.988	148.6	257.6	103.2
#176	0.991 ± 0.026	0.925 ± 0.198	83.6 ± 6.4	341.8 ± 9.2	311.8 ± 8.4
C/2015 D4*	0.862	0.989	77.3	314.7	305.8
#191	0.952 ± 0.021	0.958 ± 0.19	132.4 ± 3.4	28.8 ± 5.5	317.4 ± 9.3
C/1852 K1	0.905	1.0	131.1	37.2	319.3
#206	0.677 ± 0.037	0.969 ± 0.094	148 ± 2.1	109.4 ± 6.1	158.9 ± 7.4
C/1911 N1	0.684	0.996	148.4	110.4	158.7
#410	0.920 ± 0.018	0.998 ± 0.111	178.2 ± 0.9	143.8 ± 4.1	90.9 ± 2.2
C/1864 N1	0.909	0.996	178.1	151.6	97.7
#428	0.626 ± 0.062	0.966 ± 0.081	149.3 ± 3.0	104.8 ± 8.2	275.1 ± 14.8
C/1846 J1	0.634	0.990	150.7	99.7	264.0
#502	0.796 ± 0.029	0.960 ± 0.104	152.8 ± 3.0	127.4 ± 5.4	256.2 ± 5.6
C/1961 T1*	0.681	0.992	155.7	126.6	247.4
#512	0.988 ± 0.005	0.902 ± 0.141	106.2 ± 2.9	2.2 ± 7.5	45.3 ± 5.4
C/1879 M1	0.896	1.0	107.0	3.74	47.5
#524	0.916 ± 0.011	0.961 ± 0.11	115.4 ± 2.2	147.4 ± 3.2	214.4 ± 1.4
C/1975 T2	0.838	0.985	118.2	152.0	216.8
#531	0.985 ± 0.008	0.941 ± 0.123	123.2 ± 2.0	198.1 ± 3.4	48.7 ± 2.9
C/1853 G1*	0.909	0.989	122.2	199.2	43.0
#533	0.851 ± 0.063	0.958 ± 0.145	170.9 ± 2.8	312.1 ± 10.4	291.9 ± 10.8
C/1964 N1	0.822	0.985	171.9	290.8	269.9
#535	0.514 ± 0.031	0.999 ± 0.07	138.5 ± 1.7	89.1 ± 5.6	312.9 ± 2.3
C/1939 H1	0.528	0.991	138.1	89.2	312.3
#545	0.724 ± 0.015	0.966 ± 0.053	97.5 ± 1.0	245 ± 2.4	149.4 ± 1.0
C/1871 V1*	0.691	0.995	98.3	242.9	148.9
#705	0.781 ± 0.026	0.950 ± 0.084	103.8 ± 1.8	121.8 ± 4.4	166.3 ± 3.0
C/2002 Y1	0.714	0.997	103.8	128.8	166.3

Note. Median observed shower orbital elements with dispersions and associated parent body as found in P. Jenniskens et al. (2021). An asterisk indicates uncertain parent/shower associations. Comet elements from JPL Horizons Small-Body Database.
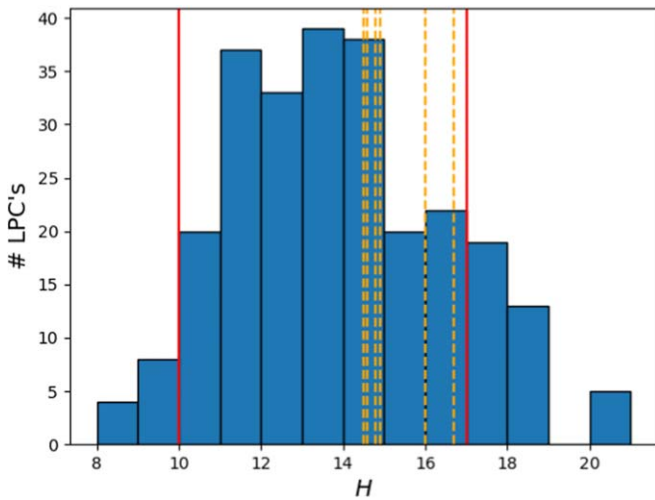

Figure 1. Distribution of H values for LPCs from JPL's Small-Body Database. Solid red lines denote assumed cutoff values for comets with undefined bare nucleus magnitudes. Dashed orange lines indicate nominal H values for the six comets in our sample that have this property constrained.

the observing location. Obscode G37, corresponding to the Lowell Discovery Telescope in Happy Jack, Arizona, was used in our analysis.

2.3. Comet Observability: Defining the Sweet Spot

Our ideal search area is when the comet is at opposition, approaching perihelion (true anomaly $>180°$), and where it has an apparent brightness fainter than achieved in routine observations by ongoing asteroid surveys ($V \sim 22$), but still within reasonable limits for current targeted or future wide-field surveys ($V < 25$). Figure 2 offers a visual example of what the sweet spot looks like in one of our simulations.

Comets brighter than $V = 22$ would have already been discovered by existing surveys such as Pan-STARRS or the Zwicky Transient Facility (B. Flaugher et al. 2015; E. C. Bellm et al. 2018; K. C. Chambers et al. 2019). The upper limit on V corresponds to the approximate single image depth of LSST (Z. Ivezić et al. 2019). Opposition is where the comet appears brightest as seen from Earth. Comets are typically discovered while they are approaching perihelion because they become brighter as they get closer to the Sun. We exclude outbound
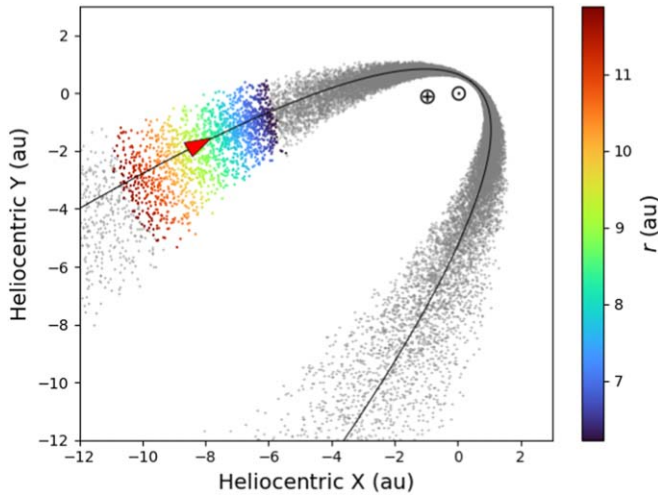
Figure 2. The observability sweet spot for the Aurigids (IAU shower 206) of comet C/1911 N1 (Kiess) for the date of 1909 March 27, when its parent comet was 9 au from the Sun. The red arrow marks the comet position and direction of motion at that time. $\odot$ is the Sun, and $\oplus$ is Earth. Gray circles are the synthetic comets on Aurigid-type orbits. The region with colored symbols highlights the heliocentric distance range that would be observable for a comet with $H = 14$.

(post-perihelion) comets because they would already have been discovered when their apparent brightness was high due to close proximity.

Comet brightness is due to the size of the nucleus, but also the rate at which dust and gas are ejected. Comets are known to begin sublimating water ice at ∼5 au (F. L. Whipple 1950; D. Jewitt et al. 2007), but they can also exhibit activity at distances as far out as ∼35 au, where activity is driven by sublimation of volatiles other than water or by other physical processes of ejection (D. Jewitt et al. 2021).

Because the behavior of the comet can vary, we adopt a conservative approach by assuming that the comet is inactive at discovery. The assumption of a bare comet nucleus gives us conservative estimates of the comet's V at any given r, as any increase in the comet's activity would make it brighter and easier to find. The V of an inactive comet is derived from H. The H of the comet nucleus is a parameter passed into OpenOrb that is one of the predominant contributors to the variance of outcomes in our simulations.

Only 6 of the 17 comets we modeled have observed H values with specified uncertainties. Five of these six comets had H values listed in the JPL Small-Body Database. Here we use the term H interchangeably with the nuclear magnitude $M2$, as is often used for comets. The H values for comets with measured nuclear magnitudes are listed in Table 2. The absolute magnitude for C/1983 H1 (Iras-Araki-Alcock) was published by O. Groussin et al. (2010).

To determine the suitable range of H for comets with no known values, the JPL Small-Body Database was searched for hyperbolic or parabolic comets with known H values. From these 259 comets, we obtained a distribution of nuclear magnitudes (Figure 1) to inform a plausible range of H. Just over 82% of H values in this distribution fall into the 10–17 mag range, bounds that are then used to define the range of H for showers with unconstrained nuclear magnitudes. Cometary albedos fall within a typical range of 0.04–0.06 (M. M. Knight et al. 2023); thus, $H < 17$ corresponds to diameters great than ∼1 km and would be considered

potentially hazardous. The drop-off in numbers above $H = 17$ is thought to be real, with relatively few comets known to have a diameter much less than 1 km.

Assuming a viewing geometry that puts the comet at opposition, we solved for the range of r that would put the comet within our brightness limits (P. L. Lamy et al. 2004):

$$V = H + 5\log_{10}(r\Delta) - 2.5\log_{10}q(\alpha), \qquad (1)$$

where V is visual magnitude, H is the comet's absolute magnitude, r is the comet's heliocentric distance, Δ is the distance between the object and Earth, and $q(\alpha)$ is the phase integral at solar phase angle α. Assuming that the comet nucleus is an inactive, Lambertian surface, the phase integral is given by (C. T. Whitmell 1907)

$$q(\alpha) = \frac{2}{3}\left[\frac{(\pi - \alpha)\cos\alpha + \sin\alpha}{\pi} \right]. \qquad (2)$$

Because searches would be optimized when the object is at opposition ($\alpha = 0°$), the phase integral reduces to $\frac{2}{3}$. Δ in terms of heliocentric distance becomes $r - 1$, providing a way to calculate visual magnitudes solely as a function of H and r.

2.4. On-sky Ephemeris

We created synthetic comets by generating 1000 random clones for each 1° of true anomaly, resulting in 360,000 random clones for each shower. Each clone is pulled from a uniform random sample of the shower's five Keplerian orbital elements. A uniform distribution inflates our calculated search regions but provides conservative estimates on where to begin searching, a method that can be refined with future work. We filtered out synthetic comets that were not on LPC-like orbits and fell outside of the observability constraints.

We computed an ephemeris for each synthetic comet using OpenOrb (utilizing the COT coordinate type). For the purpose of this test, observatory code G37 (Lowell Discovery Telescope) was used. OpenOrb returns epoch J2000 R.A. and decl. positions in the topocentric equatorial coordinate system.

The dates for ephemeris generation were dictated by the parent comet. The date selected was based on the parent comet's heliocentric distance from the Sun on its previous passage through the solar system. We pulled dates from the JPL Small-Body Database corresponding to when the parent comet was at heliocentric distances that put its V within the range defined earlier, $22 \leqslant V \leqslant 25$. We generated an ephemeris for each date corresponding to those r values. This approach placed the synthetic comets in what was the parent comet's path on its last perihelion passage. This allows us to constrain the parent comet's location with respect to the synthetic comets.

Observable synthetic comets with LPC-like orbits, along with the shower's parent comet, were plotted by their position on sky in R.A. and decl. Figure 3 provides an example of a search area on the sky for C/1939 H1 (Jurlof-Achmarof-Hassel). The figure is a visualization of observable synthetic comets (gray circles) simulated using median orbital elements and their dispersions from shower #535, $H = 14$, on the date the parent comet was at 8 au (1937 May 16).

The R.A. and decl. positions depend on the position of Earth in its orbit and the part of the comet orbit that is selected from the assumed range of brightness.

Table 2
Mean Simulation Results by Meteor Shower

	Shower	H	$\delta_l \pm \sigma_l$ (deg)	Ψ (deg)	ψ_l (%)	$\delta_r \pm \sigma_r$ (au)	$\bar{K}_s$ (arcsec minute^{-1})	$\bar{K}_p$ (arcsec minute^{-1})	$\bar{\theta}_s$ (deg)	$\bar{\theta}_p$ (deg)
Unknown H showers	6	10–17	1.14 ± 1.39	<4.67	24	1.43 ± 1.42	0.225	0.229	150.3	153.2
	23*	10–17	2.85 ± 0.64	2.16	132	2.41 ± 1.75	0.146	0.153	189.5	188.0
	175	10–17	1.65 ± 0.65	3.57	47	2.44 ± 1.82	0.180	0.173	163.2	162.8
	191	10–17	3.33 ± 1.28	5.92	56	2.47 ± 2.35	0.248	0.206	183.7	183.8
	206	10–17	0.83 ± 0.41	4.09	20	2.35 ± 1.98	0.187	0.172	191.0	191.8
	410	10–17	0.25 ± 0.04	0.30	83	1.70 ± 1.75	0.162	0.155	176.7	175.4
	428	10–17	1.70 ± 0.83	5.65	30	2.60 ± 2.00	0.183	0.184	170.0	171.7
	512	10–17	1.48 ± 0.88	7.10	21	2.05 ± 1.81	0.190	0.184	178.6	174.5
	531*	10–17	1.81 ± 0.84	3.25	56	2.15 ± 2.23	0.216	0.202	172.7	181.1
	535	10–17	0.53 ± 0.34	2.48	21	2.13 ± 1.81	0.192	0.187	203.1	204.0
	545*	10–17	1.00 ± 0.33	1.62	62	1.26 ± 0.89	0.212	0.225	177.7	179.7
	Mean		1.51 ± 1.19	3.71	50	2.09 ± 1.89	0.195	0.188	177.9	179.7
Known H showers	145	14.9	0.57 ± 0.43	2.62	22	0.44 ± 0.20	0.313	0.302	148.4	146.9
	176*	14.8	13.89 ± 5.06	10.60	131	2.28 ± 1.57	…	0.253	…	169.1
	502*	16.7	2.75 ± 1.23	3.68	75	0.88 ± 0.51	0.312	0.301	155.0	156.0
	524	14.6	1.51 ± 0.51	2.09	72	0.78 ± 0.55	0.203	0.188	184.0	184.5
	533	16.0	2.92 ± 0.48	2.28	128	0.98 ± 0.60	0.182	0.189	176.1	169.7
	705	14.5	1.22 ± 0.72	4.03	30	1.67 ± 1.09	0.239	0.204	250.0	248.9
	Mean		1.70 ± 1.12	4.22	76	0.96 ± 0.80	0.250	0.237	182.7	181.2
Overall average			1.51 ± 1.19	3.89	59	2.05 ± 1.87	0.212	0.204	179.4	179.5

Note. Given are the average distance of the parent comet from the synthetic comet trend line (δ_l), synthetic comet cloud width (Ψ), average difference in heliocentric distance between the comet and particles on the line (δ_r), standard deviation (σ_l and σ_r) of those calculations for all 17 showers, mean nonsidereal rate for synthetic comets ($\bar{K}_s$) and their parents ($\bar{K}_p$), and direction of motion measured in degrees east of north for synthetic comets ($\bar{\theta}_s$) and their parents ($\bar{\theta}_p$) across all simulations ($n = 850$). Ψ is the distance from the trend line to the outside of the cloud that encompasses 99.7% of all synthetic comets. ψ_l presents δ_l as a percentage of Ψ. δ_r is the difference between the heliocentric distance of the parent comet and the heliocentric distance of synthetic comets in the 1° bin at the point on the line where δ_l is measured. σ_l and σ_r measure how widely values of δ_l and δ_r are dispersed from the mean. $\bar{K}_s$ and $\bar{\theta}_s$ are the mean rate and angle (measured east of north) for all synthetic comets inside a 3° FOV around the parent comet across all simulations. $\bar{K}_p$ and $\bar{\theta}_p$ are the mean rate and angle of the parent comet pulled from the JPL Small-Body Database for the date of each simulation. An asterisk indicates uncertain parent/shower associations.
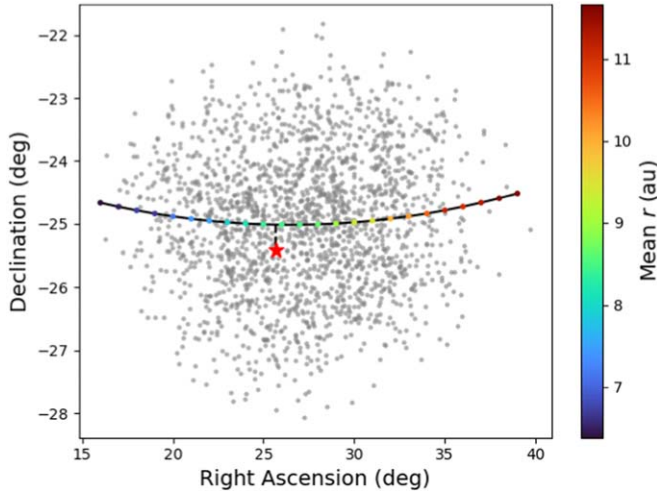

Figure 3. Case study for the shower associated with comet C/1939 H1 (Jurlof-Achmarof-Hassel), the position of which is shown by a red star. Colored circles on the line represent the mean r of synthetic comets in 1° bins along the line. Its δ_l is 0°40 and its δ_r is 0.39 au in this simulation.

To help determine the offset in position between the parent comet and the most likely position of the synthetic comets, we fit a second-order polynomial to the R.A./decl. positions of the synthetic comets (Figure 3). This line was oriented along the longest axis of the synthetic comet field, i.e., the R.A. or decl. coordinate that displayed the greatest range. The line provides a mean representation of synthetic comet positions within the cloud, as well as a reference point to compare the position of the parent comet.

An important fact to underscore is that our modeling is only attempting to show that the shower can serve as a guide to where the comet may be in the sky. It does not take into consideration viewing geometry (e.g., solar elongation), which would determine whether any particular patch of sky can be observed from Earth on a given night.

3. Results

3.1. Size and Shape of the Search Area

The dispersions in Table 1 are the standard deviation of orbital elements for measured meteors in each shower, after removing the effect of nodal precession (P. Jenniskens 2023). The projected area on sky for a set of synthetic comets is dependent on these measured dispersions. Figure 4 is a representation of our 17 showers. Some search areas are diffuse; others are compact.

The comet position is plotted as red stars. In general, the comet positions were found to be projected inside the cloud of synthetic comets, despite the meteoroid stream only having been sampled in Earth's path. The parent comets of two showers (#23 and #533; Figure 4) are found right on the edge of the projected cloud.

The one clear exception is the case of shower #176, labeled in yellow, where the proposed parent comet C/2015 D4
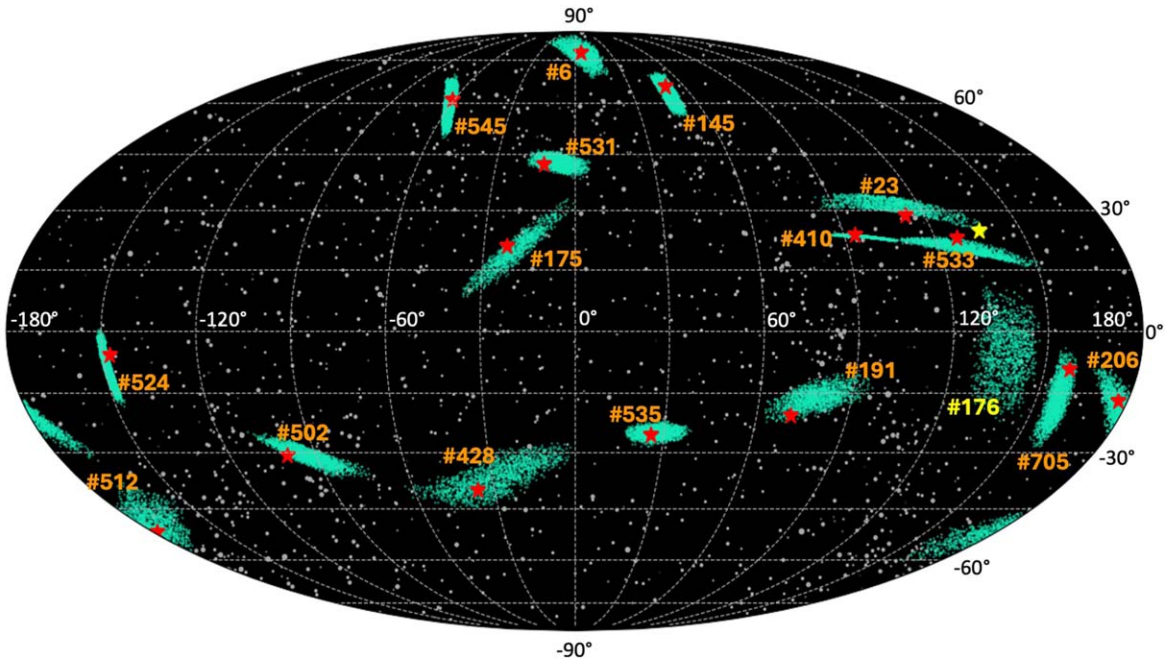
Figure 4. A celestial sphere projecting all 17 synthetic comet clouds, with the position of the parent comet plotted as a red star. Orange text denotes the shower number used to generate the cloud.

projects at a higher decl. than the cloud. This is also our most dispersed shower, with a high amount of precession of the elements in Earth's path due to a low inclination of the orbit. The disagreement could mean that C/2015 D4 is not the parent body of shower #176, or that the stream extends well beyond the part of the stream observed at Earth as a meteor shower.

Differences in brightness between the parent comet and synthetic comets along the comet orbit are attributed to differences in heliocentric distance (Equation (1)). This defines two characteristic uncertainties: one along orbit responsible for the highest on-sky dispersion (reflecting spread along the comet orbit from variation in H), and the other perpendicular to that line (from the perpendicular dispersion of the shower).

Determining the perpendicular distance from the line to the parent comet (δ_l) gave us a representative uncertainty in on-sky position. The width of the synthetic comet cloud (Ψ) is defined as the distance from the line to the outside of the cloud that encompasses 99.7% (3σ) of all synthetic comets. Ψ was computed by calculating δ_l for each synthetic comet and using a cumulative frequency distribution of all distances to determine the 3σ width. The 3σ width is used to exclude outlying synthetic comets whose distance from the line is not representative of the rest of the distribution. We use this to express δ_l as a percentage of the width of the cloud (ψ_l) and provide a more illustrative description of where the parent comet was located with respect to the synthetic comets.

The along-orbit dispersion is a measure of uncertainty caused by the unknown comet brightness. For each $1°$ bin on the along-orbit trend line, we calculated the mean r of the synthetic comets in that bin. The difference between mean r of the synthetic comets on the line at that point and r of the parent comet (δ_r) suggests a characteristic uncertainty in r that constrained the apparent nonsidereal motion of the object, since nonsidereal motion will correlate with heliocentric distance.

Table 2 summarizes calculations of δ_l, δ_r, Ψ, and ψ_l, completed across all simulations. Results for shower #176 are not included in the calculated averages.

These numbers are also affected by the coordinate system used. One of our showers (#6) had a cloud of synthetic comets that stretched over the northern pole in several of the simulations that were run. A skewed fit line resulted in this situation. After excluding six simulations where the synthetic comet cloud stretched over the north pole out of 74 total simulations, the mean δ_l improved by $0°.11$, σ_D improved by $0°.19$, δ_r increased by $<5\%$, and σ_r increased by 0.03 au, while Ψ improved by $0°.25(5.4\%)$.

Figures 5(a) and (c) show δ_l and δ_r, respectively, as a function of heliocentric distance across all 850 simulations. The histograms in panels (b) and (d) show distributions of δ_l and δ_r, respectively, across all simulations.

3.2. The Direction of Motion for Shift-and-stack Searches

A shift-and-stack search strategy (G. M. Bernstein et al. 2004; C. Zhai et al. 2020) involves stacking a sequence of images at a specified rate and angle of motion in an effort to access fainter magnitudes. Shifting and stacking of images can be computationally intensive if bounds on the rate and angle on sky are unknown, as one would need to test all possible parameters (rates and angles).

By comparing the velocity vectors of the synthetic comets to those of the parent comets in our sample, we were able to provide useful bounds to this type of search strategy. For example, LSST will have a $3°.5$ field of view (FOV; LSST Science Collaboration et al. 2009). Mean velocity vectors of the synthetic comets inside a $3°$ FOV around the parent comet were compared to the parent's velocity vector. Table 2 summarizes the mean rates ($\bar{K}_s$) and angles ($\bar{\theta}_s$) of the synthetic comets inside the $3°$ FOV, along with the mean rates ($\bar{K}_p$) and angles ($\bar{\theta}_p$) of the parent comets across all simulations. Figure 6 depicts how the velocity vectors of the synthetic comets inside such a region compare to that of the parent.

Figure 7 shows the aggregate of all of the differences between mean rates and angles of synthetic comets and those of
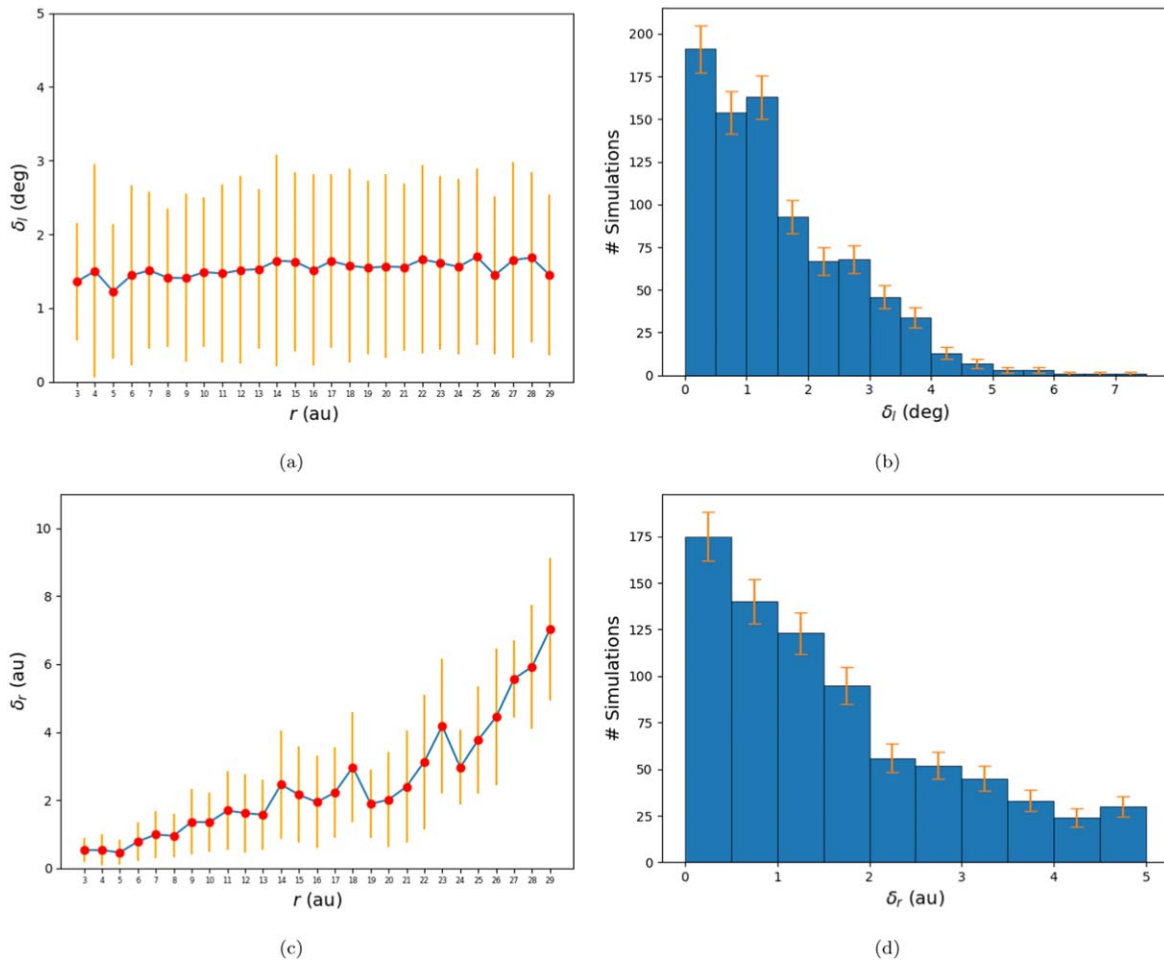
Figure 5. Line plots in panels (a) and (c) show average values of δ_l and δ_r, respectively, with standard deviations for all showers as a function of heliocentric distance. Histograms in panels (b) and (d) provide distributions of δ_l and δ_r, respectively, for all simulations across all showers. Error bars in the line plots are the standard deviations across all simulations. Error bars in the histograms are calculated as $\sqrt{N}$.

the parent comet. Approximately 96% of the parent comets were traveling at rates $\pm 0\rlap{.}''15\,\mathrm{minute}^{-1}$ and $\pm 15°$ from the mean direction of motion of the synthetic comets within a 3° FOV, defining bounds that can then be used in a shift-and-stack search for faint objects.

We estimate a quantitative reduction in this parameter space by taking the ratio of the number of bound parameters to the total number of (unbound) parameters in $d\mathrm{R.A.}/d\mathrm{decl.}$ (arcsec minute^{-1}) space. We defined the total parameter space by estimating a maximum possible rate for the synthetic comets. This allowed us to encircle all rates and position angles to be tested in a blind shift-and-stack search (Figure 8). We tested three maximum rate cases to understand their influence on the ratio of bound parameters to total parameters: the maximum rate across all simulations ($1\rlap{.}''06\,\mathrm{minute}^{-1}$); a maximum rate of $0\rlap{.}''400\,\mathrm{minute}^{-1}$, which excludes fast-moving outliers and encompasses 763 ($\sim$90%) of the mean rates found in the 850 simulations; and the maximum simulated rate at heliocentric distances greater than 15 au ($0\rlap{.}''235\,\mathrm{minute}^{-1}$). This last test focuses on faint, slow-moving objects where searches would likely be conducted. A total of 341 ($\sim$40%) of our simulations fell into this category.

For each of these cases, we added another $0\rlap{.}''15\,\mathrm{minute}^{-1}$ to set a limit on the maximum allowed rate. This defined the total possible parameter space to be searched. For each simulation

we then calculated the area in a wedge $\pm 15''\,\mathrm{minute}^{-1}$ and $\pm 15°$ centered on the mean rate of each shower (Figure 8). This wedge represents the parameter space to be tested when conducting a shift-and-stack search for a specific parent body.

When the upper bound was based on the maximum rate found in our simulations (first case), we found that the parameter space was reduced by at least 96.4%. This maximum rate is not necessarily representative of our entire sample because outliers inflate the size of the allowable parameter space, thus deflating the computed ratio. When the upper bound was based on a maximum rate of $0\rlap{.}''400\,\mathrm{minute}^{-1}$ (second case), we found that the parameter space was reduced by at least 93.4%. Finally, the parameter space was reduced by at least 92.1% for simulations at heliocentric distances greater than 15 au (third case). This reduction in parameter space of over 92% would decrease the computation time by about an order of magnitude when conducting shift-and-stack searches.

3.3. The Additional Warning Time and Distance from Earth

To address the potential for additional impact warning time provided by this method, we backward-integrated our parent comets from their dates of first observation to the date where $V = 25$. V was calculated from Equation (1) by using the r and Δ of the object on dates prior to discovery. This allowed us to
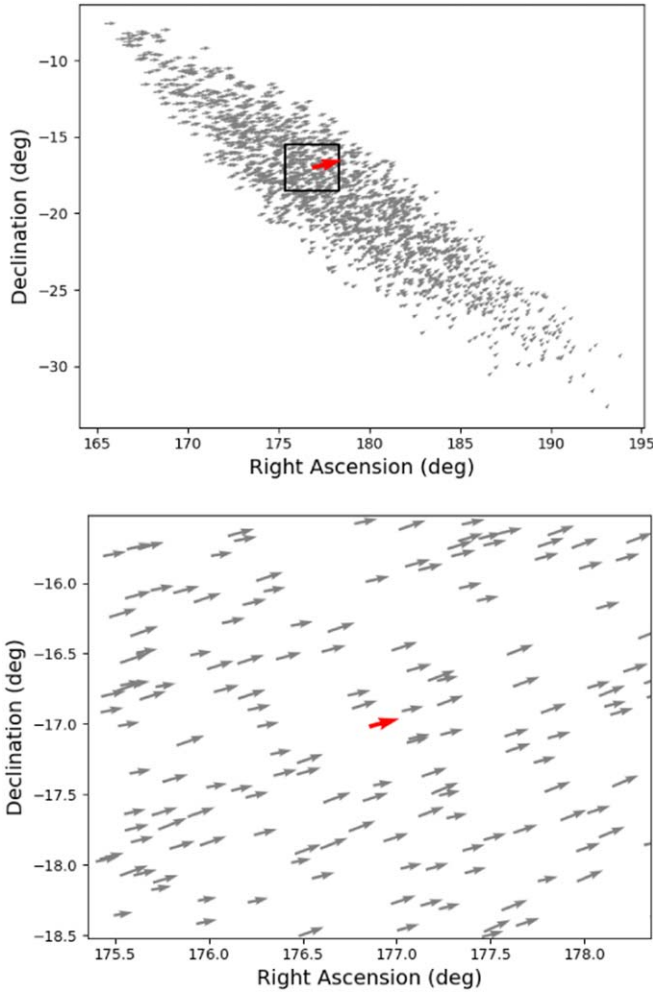
Figure 6. The top panel shows velocity vectors for each observable synthetic comet in a simulation with shower #206 (the Aurigids) on 1909 July 31. The parent comet's velocity vector is represented with a red arrow. The black box is a 3° FOV region of the search area centered around the parent comet's position and represents the FOV of a wide-angle sky survey. The bottom panel is a close-up of this region, showing that velocity vectors of synthetic comets are representative of the velocity vector of the parent comet. The mean rate of synthetic comets in this 3° region is $0\rlap{.}''144 \pm 0\rlap{.}''016$ minute^{-1}, and the rate of the parent comet is $0\rlap{.}''145$ minute^{-1}.

calculate V of inactive comet nuclei, consistent with an assumption made throughout our modeling.

The difference between the discovery date and the date where $V = 25$ informs the additional warning time provided if an LPC on a potential Earth-intersecting orbit were discovered using this method. Table 3 provides calculations of the additional years before discovery and the distance from Earth if these LPCs were discovered at $V = 25$ for objects with $10 \leqslant H \leqslant 17$. In that metric, the largest comets ($H = 10$) would be discovered farther out in the solar system and provide over 12 yr additional warning time, while the smallest comets ($H = 17$) would still provide over a year to determine and execute mitigation strategies.

4. Discussion

4.1. Uncertainty of the Search Area

While we found that the calculated search areas capture well the location of the comet for showers with known parent
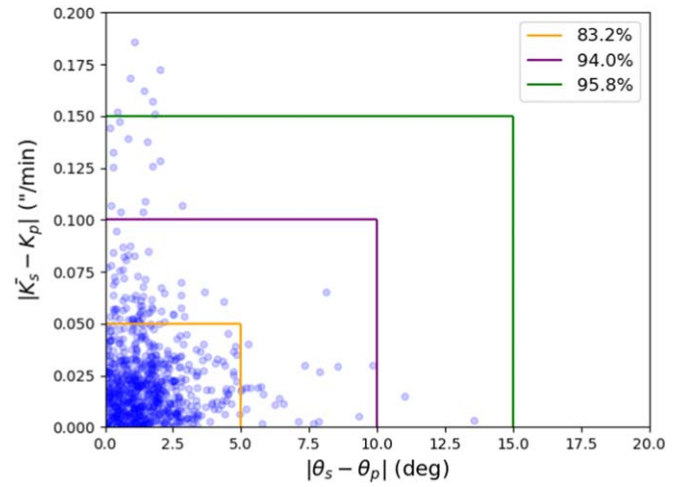

Figure 7. Differences between mean synthetic comet rates and angles and those of the parent comets inside a 3° FOV search region encompassing the parent comet. The legend shows the percentage of total simulations ($n = 850$) that fall within bounds of $0\rlap{.}''05$ minute^{-1} and 5° (yellow), $0\rlap{.}''1$ minute^{-1} and 10° (purple), and $0\rlap{.}''15$ minute^{-1} and 15° (green).
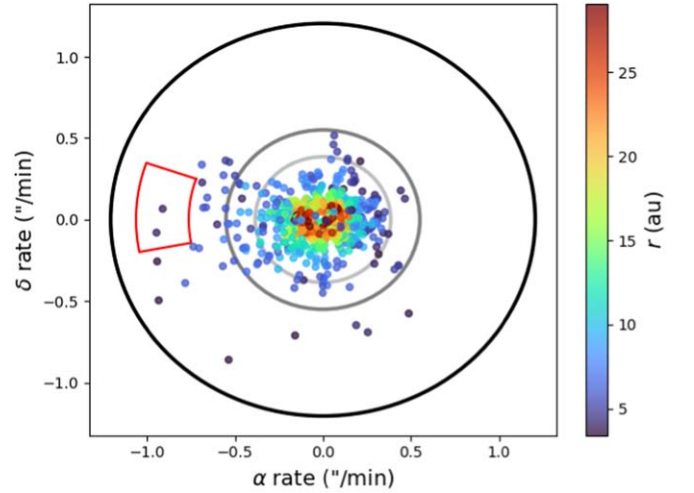

Figure 8. R.A./decl. rates (arcsec minute^{-1}) for each simulation ($n = 850$) color-coded by r. The outer circle represents case 1; the middle circle, case 2; and the inner circle, case 3. The example wedge sets bounds on the rates and angles for a shift-and-stack search in the region defined by shower #531 with $H = 14$ and $r = 4$ au, based on bounds discussed in Section 3.2 ($\pm 0\rlap{.}''15$ minute^{-1} and $\pm 15°$). These bounds reduce the parameter space by 96.5% for this simulation.

Table 3
Additional Warning Time Provided and Distance from Earth at Discovery

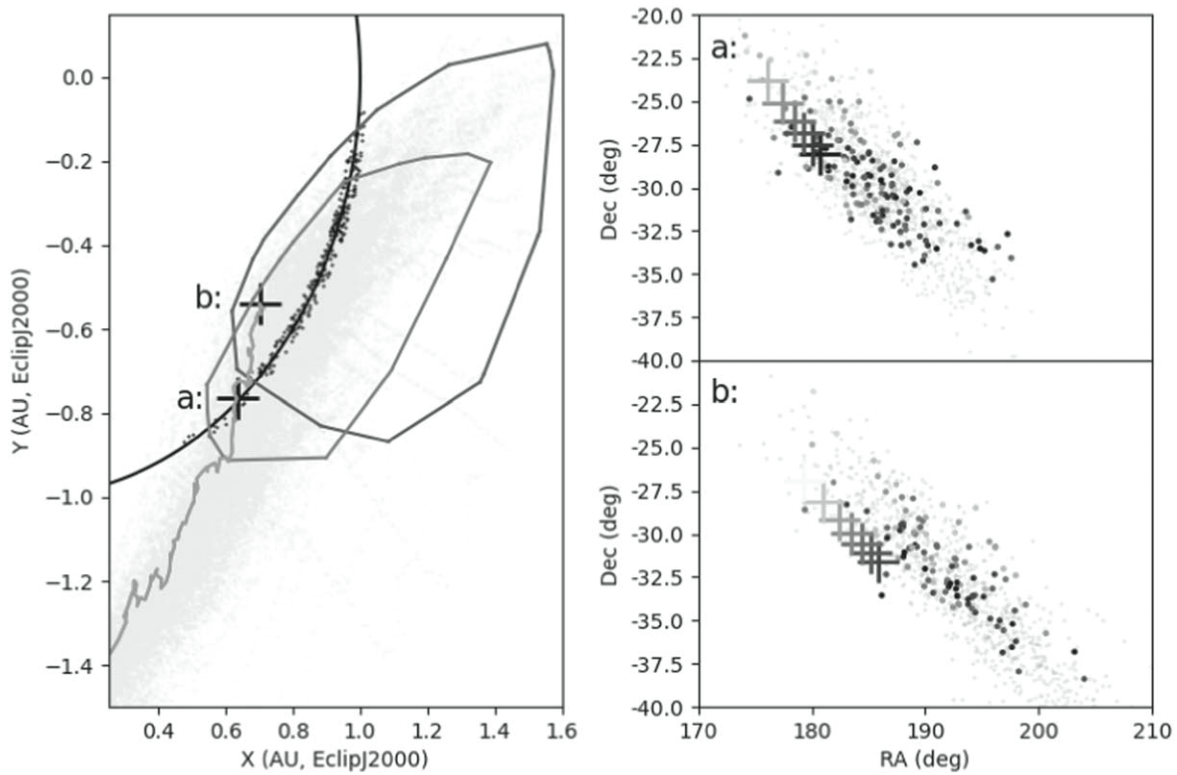| H	Years Warning	Δ (au)
10	12.6	28.9
11	8.8	23.1
12	6.4	18.1
13	4.6	14.5
14	3.3	11.5
15	2.4	9.2
16	1.7	7.5
17	1.2	5.9
Mean	5.1	14.8

Figure 9. Locations of meteoroid and comet node crossings in the ecliptic plane (left) and the projected location of comet and meteoroids on the sky at two epochs (right; see text for details) for a simulation of shower #206 (the Aurigids). The parent body is marked in both panels with plus signs. The locations of approximately 95% of meteors crossing within 500 yr of the comet at epochs "(a)" and "(b)" are encircled (left), or appear in light gray (right). The subset of Earth-intersecting ejecta is shown in black on the left and in gray scale graded by magnitude on the right. On the right, the comet's location is shown at vernal equinox for all the years it takes to traverse from $V = 25$ to $V = 22$.

bodies, there are some matters that can change the search area in other cases. We already mentioned that our method only considers the dispersion of the meteoroid stream in Earth's path, not the full dispersion of the stream. The methodology assumes that the orbital elements of a meteoroid stream are similar to those of the parent body itself. It also assumes that the meteor shower elements are independently distributed, each characterized by only a median and dispersion, and that Keplerian orbits provide a good approximation when backing up the particles from their node to some previous time. These assumptions would be fraught for short-period comets ($P < 200$ yr), where planetary encounters and resonances might be expected to alter the parent body's orbit significantly from the shower on short (decadal) timescales, but they seem reasonable for LPCs.

Even for LPCs, the actual distributions of orbital elements in the meteor stream are not Gaussian and are likely correlated, so that independent Gaussian deviates may not adequately represent the location of the cloud on the sky. This comes into play mainly for low-inclined orbits that precess at a fast rate.

Finally, the dispersion of orbital elements may not adequately represent the measured dispersion of orbits defined by the radiant and velocity of meteors in a shower (P. Jenniskens et al. 2021). We conducted simulations starting from radiant and speed distributions to see whether this would provide any benefit in terms of generating smaller clouds and therefore smaller search regions on sky. We found that both approaches gave similar results: 57% of these radiant-derived particles were distributed in somewhat smaller clouds, and 43%

resulted in larger clouds. The clouds from these radiant-derived elements were at best ~50% smaller and at worst 300% larger than orbital element generated clouds, but overall there was not a systematic difference. Because of that, we present results here using the median Keplerian orbital elements and their dispersions as shown in Table 1.

4.2. Separate Evolution of Comet and Its Meteoroid Stream

Orbits will be perturbed from the Keplerian orbits during perihelion crossing, and over long periods of time this can create a stream in Earth's path that does not fully describe the extent of the stream away from Earth's orbit. The method failed for shower #176, if the proposed parent comet is indeed the parent body of that stream.

We performed numerical simulations of LPC dynamical evolution to investigate whether the comet orbit stays among the meteoroid orbits over the age of the observed streams (S. Pilorz et al. 2023). Examination of the loci of nodal crossings for the parent body and ejecta cloud shows that the comet has a node within the cloud's nodes, though both undergo nodal progression and stochastic wandering.

Figure 9 shows results from simulations of Shower #206 (the Aurigids), at two different epochs. For those simulations, a model for the parent comet C/1911 N1 (Kiess) was created for times between 60 kyr ago and the present, the timescale on which LPC ejecta are thought to disperse. It was found by performing backward integration followed by forward integration of several perturbations of the current observed elements, from which the variant was selected whose forward integration resulted in present-day orbital elements most similar to the

Table 4
Orbital Elements and Standard Deviations of Meteor Shower #16 (σ-Hydrids), from P. Jenniskens (2023)

	Value	Dispersion
q	0.257 au	± 0.0437 au
e	0.986	± 0.0596
i	128°8	$\pm 3°72$
ω	119°3	$\pm 7°15$
Ω	76°6	$\pm 8°30$

observed, allowing a period between 250 and 4000 yr. Numerical integrations were then performed of ejecta released during selected perihelia of this model comet, following the general method of J. Vaubaillon et al. (2005). In this case, 300 ejecta were released uniformly in time when the comet was within 3 au of the Sun, with velocities uniformly within 1–$10\,\mathrm{m\,s^{-1}}$ and random directions over the lit face.

The left panel of Figure 9 shows the loci of all node crossings of the cloud of 300 particles in ecliptic J2000 coordinates, along with the parent body at two epochs marked "(a)" and "(b)." The trajectory of the comet's node location is drawn as a solid curve, and effects of nodal progression and stochastic wandering are apparent. The plus signs show the locations of the node at an epoch near Earth crossing and a later epoch at which it is inside Earth's orbit. Polygons enclose approximately 95% of the ejecta that crossed the node within 500 yr of the comet's crossing at each epoch. The subset of these that intersect Earth's orbit, shown with black circles, are taken to be what an observer at that epoch would use to model the stream orbital elements.

The right panels of Figure 9 show the result of numerically integrating that subset of points backward individually, to locations on their inbound orbits at which they would have apparent magnitudes within $22 < V < 25$, with the end magnitude for each point chosen randomly within that range. Those magnitudes correspond to ranges of approximately 12–25 au and take the comet approximately 7 yr to traverse. The seven plus signs are the comet's R.A./decl. at vernal equinox each year for those 7 yr. The plus signs and circles are shaded by their apparent magnitudes, with black corresponding to $V = 25$ and lighter gray corresponding to $V = 22$. The particles' locations move from the lower right to upper left of the cloud as they approach.

This figure shows the typical behavior we observe: the comet's location on the sky lies within the cloud of points at epochs where its node is near 1 au but lies at the edge of the cloud at epochs where the node has drifted inward.

The numerical simulations indicate that even for meteors ejected 60 kyr in the past the position of the comet remains within or at the edge of the stream. Its location on the sky is within the cloud of the subset of ejecta that cross Earth's orbit and would correspond to the sampled distributions described in Section 2.3.

4.3. Comet Nishimura

C/2023 P1 (Nishimura) was an LPC discovered by amateur astronomer Hideo Nishimura with a digital camera in 2023 August (H. Nishimura et al. 2023). The comet was very low on the horizon and escaped automatic detection by sky surveys. In combing through sky survey data after discovery of comet Nishimura, serendipitous observations were found in Pan-
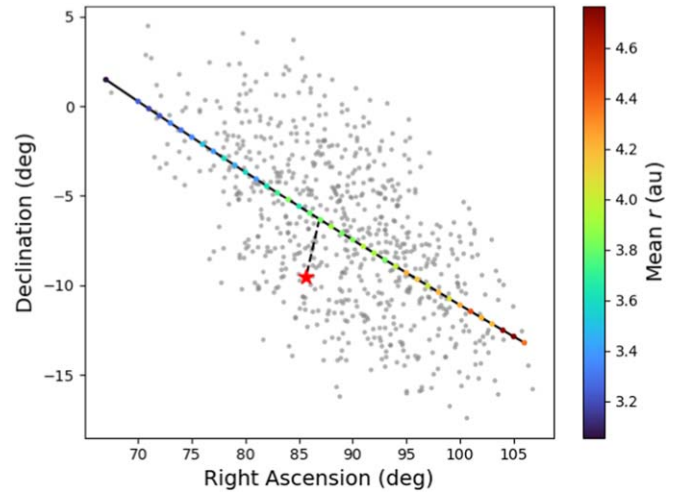

Figure 10. Search area on sky for shower #16 (σ-Hydrids) on 2023-01-19.326034 (UT). The synthetic comets in this simulation have an assumed $H = 16$. Its parent comet, C/2023 P1 (Nishimura), is represented by the red star. The model results show $\delta_l = 3°43$, $\Psi = 8°25$, $\psi_l = 42\%$, and $\delta_r = 0.24$ au.

STARRS data dating back to 2023 January (R. Weryk 2023). Comet Nishimura is also a proposed parent body of the σ-Hydrids meteor shower (Q. Ye & J. Graves 2023). This presented an opportunity to test our modeling on direct observations of a newly discovered LPC with an observed meteor shower.

There are no published estimates of comet Nishimura's absolute magnitude, so we ran simulations across the range of H used for the previous simulations ($10 \leqslant H \leqslant 17$). Using the orbital elements of the σ-Hydrids, their measured dispersions (Table 4), and an assumed H, synthetic comets were created and ephemerides were calculated with OpenOrb using obscode F52 (Pan-STARRS 2, Haleakala) for the date of the earliest Pan-STARRS detection (2023-01-19.326034). From the JPL Horizons Small-Body Database, the comet was determined to be 4.0 au from the Sun at that time. This provided a basis to bound the heliocentric distance of synthetic comets and set observability to be those with $3 \leqslant r \leqslant 5$ (1 au on either side gives a smaller cloud of potential positions) and on their inbound trajectory.

Figure 10 provides a visualization of the search region on sky produced by the σ-Hydrids meteor shower with an assumed $H = 16$. Comet Nishimura's position on 2023-01-19.326034 (UT) was pulled from the Pan-STARRS observation. We found δ_l to be 3°43, Ψ to be 8°25, and δ_r to be 0.24 au. The comet fell at a ψ_l of 42%. We obtained a range for δ_l of 2°98–3°59 across all H values.

Figure 11 shows a distribution of the visual magnitudes of observable synthetic comets from the modeling with $H = 16$. Reported G-band magnitudes from pre-covery images on 2023 January 19 were between 21.24 and 21.64 in four observations (R. Weryk 2023). The distribution of V for each simulation was where we saw the largest variation due to H. $H = 10$ produced synthetic comets with $14.8 \leqslant V \leqslant 17.2$, whereas $H = 17$ produced $21.8 \leqslant V \leqslant 24.2$. An $H \approx 16$ appears to be the best fit for this comet, using measurements from the observations to be a basis for the expected brightness of synthetic comets.

Our model assumes that the comet was inactive in the Pan-STARRS observations. Pre-covery images from Pan-STARRS showed that the comet was not displaying signs of activity (R. Weryk 2023). Using Nishimura's r (4.02 au), Δ (3.27 au),
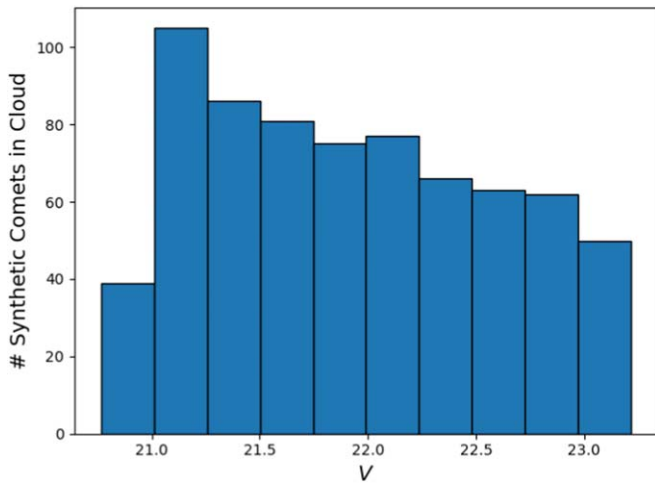
Figure 11. Histogram of visual magnitudes of synthetic comets in the search region produced by shower #16 (σ-Hydrids) as seen in Figure 10.

and α (10°.0) on the observation date, Equation (1) returns an apparent magnitude of 21.5 for an inactive comet nucleus with $H = 16$. This calculated V from the assumed H is consistent with our nominal model and direct observation.

In this exercise, known information about Nishimura helped guide which synthetic comets were observable. This highlights where the process would begin when attempting to set constraints on a blind search. When such a search for a comet is being conducted, an observer would start by knowing information about the limiting magnitude of their instrument. An estimate of the comet's absolute magnitude would need to be taken into consideration to guide the heliocentric distance range of interest for synthetic comets in the model. This could be done blindly, by using a distribution as done in this work, or possibly by using meteor shower activity to derive an estimate of H.

An instrument with a wide FOV would be in the observer's best interest. With a simulated full cloud width approaching 20° for the σ-Hydrids, an instrument with a 3° FOV would be able to capture the full width of the search region in approximately seven images. Exposure times for each image would factor into how long it might take to conduct a search in any particular region, thereby allowing observers to assess the feasibility of such a search. This method can provide a starting point to select sky survey observations of interesting search regions.

4.4. The Comet Association with a Meteor Shower

Not all comets in our sample may be correctly identified as the parent bodies of given meteor showers. C/2015 D4, with an uncertain association to shower #176, showed the farthest average line distance of all showers in our analysis by ∼10°. However, with an H of 14.8 listed in the JPL Small-Body Database, the number of simulations run in the analysis for this shower was small and not enough to definitively determine whether this comet is in fact related to the meteor shower.

In a real search for parent comets, it would be likely that many objects could be detected in these large search regions. We note that the mere detection of an object in one of these regions does not imply that it is the parent body of a meteor shower. These detections will identify objects that are candidates for follow-up observations. As the orbit and

trajectory of the object are further refined, D-criterion tests can be computed to confirm or deny a parent/shower relationship.

Determining the number of objects that might "look" like the objects for which we are searching can give us insight into the probability of a false association. We used the orbits of 831 comets with "C" prefixes and eccentricities ⩽1 from the JPL Small-Body Database to quantify the possible rate of false detections. We determined which orbits intersected the simulated clouds in Figure 4. From there, we looked at which of these comets were within the brightness constraints we set for our searches ($22 \leqslant V \leqslant 25$) and moving within the velocity constraints found in our analysis. These constraints are nonsidereal rates $\pm0.''15$ minute^{-1} and position angle (east of north) $\pm15°$ of the synthetic comet's mean motion within a 3° box around the comet as it is moved through the cloud of synthetic objects.

When applying these position and velocity cuts, we found that an average of 11.4 of the 831 comets (1.4%) could be mistaken for the parent comet across all 17 showers. False probabilities were as high as 4.1% for shower #176 and as low as 0.2% for showers #545 and #541. The known population skews the size distribution toward larger objects ($H \leqslant 17$) and may not fully reflect the total comet population. Given that, this exercise shows how a large number of objects (⩾95%) detected in these regions may be ruled out based on the expected brightness and direction of motion calculated by the simulated shower.

5. Conclusions

Meteor showers can be a practical guide to dedicated searches for LPCs with the range of orbital periods 200–4000 yr. By identifying comets at an earlier stage of their approach toward Earth, this would increase the warning time to help devise and implement more effective strategies for deflecting an impact.

Our dynamical modeling shows that the parent comet and meteoroids evolve in much the same way and that in most cases the parent comet is expected to be found in projection among the synthetic comets sampled from the observed meteor shower in Earth's path.

Indeed, known parent comets of meteor showers are mostly found inside those search areas. On average, the parent comets would have been discovered at a distance of $1°.51 \pm 1°.19$ from the mean positions of a cloud of synthetic comets. Of these comets, 50% fell at $\delta_l = 1°.18$ ($\psi_l = 30.3\%$), 70% fell at $\delta_l = 1°.91$ ($\psi_l = 47.9\%$), and 90% fell at $\delta_l = 3°.29$ ($\psi_l = 84.5\%$).

The uncertain brightness of the potential parent body makes the search areas elongated along the projected comet orbit on the sky. The mean heliocentric distance of synthetic comet particles from the trend line was 2.09 ± 1.89 au for showers with unknown H values and 0.96 ± 0.80 au for showers with known H values.

The search areas calculated from the meteoroid stream dispersions at Earth are feasible for dedicated searches. The δ_l values calculated in this study confirm the feasibility of using wide-angle sky surveys, such as LSST (3°.5 FOV) or DECam (2°.2 FOV), to discover unknown parent comets of LPC meteor showers.

The meteor showers also constrain the motion of the parent comet on sky. Within a 3° region, the parent comets were traveling within $\pm0.''15$ minute^{-1} of the mean rate and $\pm15°$ of

the mean position angle of synthetic comets in that region. With typical seeing conditions of $\sim 1''$ and comets traveling $0''.2$ minute^{-1} or less, the feasibility of discovery is not likely to be influenced by trailing losses. These values indicate that exposures of up to 5 minutes can be taken before trailing losses would affect the discovery of these objects.

Detecting LPCs at their faintest can provide years' worth of warning time for a potential impactor. The warning time can increase to over 10 yr by detecting the largest objects with this method. For smaller objects, the additional year or two gained by earlier detection would still give significantly more time to mitigate an impact.

This method successfully used the σ-Hydrids to create a search region matching the location of comet Nishimura in precovery images taken 8 months prior to its discovery.

5.1. Future Work

This method can now be applied to LSST observations. Expanding our knowledge and catalog of small bodies in the solar system is a main science driver of LSST (Z. Ivezić et al. 2019). It is predicted that LSST will more than double the current comet population from ~ 4000 to $\sim 10,000$ objects (LSST Science Collaboration et al. 2020). LSST simulations can be run to determine how many parents of these LPC meteor showers may be discoverable with this survey. This information could then be used to prioritize specific search regions within the LSST data stream.

The ideal search strategy would be to push the detection limits of LSST by employing a shift-and-stack search method. The meteor shower informs which region of the sky the parent will be in, as well as its speed and direction of motion. Warning time in the case of a PHO is also improved by pushing the limits of detection beyond that of a single image exposure.

The LSST data stream will generate ~ 400 alerts per visit associated with moving objects.[4] Alerts are distributed within 60 s of camera readout to designated alert brokers, which are then accessible by the scientific community.[5] With 1000 visits per night, the sheer volume of alerts generated in a single night will be overwhelming. In addition to the number of alerts generated by these detections, faint discoveries barely above background noise in LSST images will likely escape automatic detection algorithms.

Knowing which regions of sky will contain objects of interest will help prioritize analysis steps. Our method will guide searches for objects in individual exposures that were missed in automated detection routines and can be used to probe deeper with image stacking techniques that will not be part of the standard LSST data processing pipeline.

As a first step, P. Jenniskens (2023) determined the orbital elements and dispersions of 247 LPC meteoroid streams, most from unknown LPC parents. The development of a website to guide searches for these objects is in the early development phases.

As a future improvement on the method outlined here, we aim to determine probability densities for discovery within each shower's search region. With an average solid angle of 255 sr per region, this can highlight specific areas within the search regions that would have higher probability for success. One method to assign probability would be to weight the

synthetic comets by the inverse of their orbital period. Longer-orbit synthetic comets may better resemble the parent comet's orbit. This is because the measured orbits of meteor showers are often shorter than those of their parent comets, due to more frequent Earth impacts. This refinement could further narrow down the best areas to begin a search.

ORCID iDs

Samantha Hemmelgarn ⬤ https://orcid.org/0009-0006-1160-3829
Nicholas Moskovitz ⬤ https://orcid.org/0000-0001-6765-6336

References

Astropy Collaboration, Price-Whelan, A. M., Lim, P. L., et al. 2022, ApJ, 935, 167
Astropy Collaboration, Price-Whelan, A. M., Sipőcz, B. M., et al. 2018, AJ, 156, 123
Astropy Collaboration, Robitaille, T. P., Tollerud, E. J., et al. 2013, A&A, 558, A33
Bellm, E. C., Kulkarni, S. R., Graham, M. J., et al. 2018, PASP, 131, 018002
Bernstein, G. M., Trilling, D. E., Allen, R. L., et al. 2004, AJ, 128, 1364
Boe, B., Jedicke, R., Meech, K. J., et al. 2019, Icar, 333, 252
Chambers, K. C., Magnier, E. A., Metcalfe, N., et al. 2019, arXiv:1612.05560
Drummond, J. D. 1981, Icar, 45, 545
Flaugher, B., Diehl, H. T., Honscheid, K., et al. 2015, AJ, 150, 150
Ginsburg, A., Sipőcz, B. M., Brasseur, C. E., et al. 2019, AJ, 157, 98
Granvik, M., Virtanen, J., Oszkiewicz, D., & Muinonen, K. 2009, M&PS, 44, 1853
Gritzner, C., Dürfeld, K., Kasper, J., & Fasoulas, S. 2006, NW, 93, 361
Groussin, O., Lamy, P. L., & Jorda, L. 2010, P&SS, 58, 904
Harris, C. R., Millman, K. J., van der Walt, S. J., et al. 2020, Natur, 585, 357
Hunter, J. D. 2007, CSE, 9, 90
Ivezić, Z., Kahn, S. M., Tyson, J. A., et al. 2019, ApJ, 873, 111
Jenniskens, P. 2006, Meteor Showers and their Parent Comets (Cambridge: Cambridge Univ. Press)
Jenniskens, P. 2008, Icar, 194, 13
Jenniskens, P. 2023, Atlas of Earth's Meteor Showers (Amsterdam: Elsevier)
Jenniskens, P., Gural, P. S., Dynneson, L., et al. 2011, Icar, 216, 40
Jenniskens, P., Lauretta, D. S., Towner, M. C., et al. 2021, Icar, 365, 114469
Jenniskens, P., Lyytinen, E., Johannink, C., et al. 2020, P&SS, 181, 104829
Jewitt, D., Chizmadia, L., Grimm, R., & Prialnik, D. 2007, in Protostars and Planets V, ed. B. Reipurth, D. Jewitt, & K. Keil (Tucson, AZ: Univ. Arizona Press), 863
Jewitt, D., Kim, Y., Mutchler, M., et al. 2021, AJ, 161, 188
Jopek, T. J. 1993, Icar, 106, 603
Jopek, T. J., Rudawska, R., & Bartczak, P. 2008, EM&P, 102, 73
Knight, M. M., Kokotanekova, R., & Samarasinha, N. H. 2023, arXiv:2304.09309
Lamy, P. L., Toth, I., Fernandez, Y. R., & Weaver, H. A. 2004, in Comets II, ed. M. C. Festou, H. U. Keller, & H. A. Weaver (Tucson, AZ: Univ. Arizona Press), 223
LSST Science Collaboration, Abell, P. A., Allison, J., et al. 2009, arXiv:0912.0201

---

[4] https://dmtn-102.lsst.io/DMTN-102.pdf
[5] https://ldm-612.lsst.io/LDM-612.pdf

LSST Science Collaboration, Jones, R. L., Bannister, M. T., et al. 2020, arXiv:2009.07653

Mainzer, A., Grav, T., Bauer, J., et al. 2011, ApJ, 743, 156

Marsden, B., & Steel, D. 1994, in Warning Times and Impact Probablilities for Long-Period Comets, ed. T. Gehrels, M. S. Matthews, & A. Schumann (Tucson, AZ: Univ. Arizona Press), 221

Meech, K. J., & Svoren, J. 2004, in Comets II, ed. M. C. Festou, H. U. Keller, & H. A. Weaver (Tucson, AZ: Univ. Arizona Press), 317

Morrison, D. 2006, Comets and the Origin and Evolution of Life, Advances in Astrobiology and Biogeophysics (Berlin: Springer), 285

Nishimura, H., Yoshimoto, K., Masek, M., et al. 2023, MPEC, 2023–P87

Nuth, J. A., Barbee, B., & Leung, R. 2018, JSSE, 5, 197

Pilorz, S., Jenniskens, P., & Vaubillon, J. 2023, in Asteroids, Comets, Meteors Conf. (Houston, TX: Lunar and Planetary Inst.), 2484

Quintana, S. N., & Schultz, P. H. 2019, Icar, 326, 176

Rożek, A., Breiter, S., & Jopek, T. J. 2011, MNRAS, 412, 987

Rudawska, R., Matlovic, P., Tóth, J., & Kornoš, L. 2015, in Proc. of the Int. Meteor Conf., ed. J.-L Rault & P, Roggemans (Int. Meteor Organization), 185

Šegon, D., Vaubaillon, J., Gural, P. S., et al. 2017, A&A, 598, A15

Southworth, R. B., & Hawkins, G. S. 1963, SCoA, 7, 261

Tomko, D., & Neslusan, L. 2019, A&A, 623, A13

Toon, O. B., Zahnle, K., Turco, R. P., & Covey, C. 1994, Environmental Perturbations Caused by Asteroid Impacts (Tucson, AZ: Univ. Arizona Press), 791

Valsecchi, G. B., Jopek, T. J., & Froeschle, C. 1999, MNRAS, 304, 743

Vaubaillon, J., Colas, F., & Jorda, L. 2005, A&A, 439, 751

Weissman, P. R. 2007, in IAU Symp. 236, Near Earth Objects, our Celestial Neighbors: Opportunity and Risk, ed. G. B. Valsecchi, D. Vokrouhlický, & A. Milani (Cambridge: Cambridge Univ. Press), 441

Weryk, R. 2023, CBET, 5291, 1, http://www.cbat.eps.harvard.edu/iau/cbet/005200/CBET005291.txt

Whipple, F. L. 1950, ApJ, 111, 375

Whitmell, C. T. 1907, Obs, 30, 96

Ye, Q. 2016, PhD thesis, Univ. Western Ontario, https://ir.lib.uwo.ca/etd/3903

Ye, Q., & Greaves, J. 2023, CBET, 5290, 1, http://www.cbat.eps.harvard.edu/iau/cbet/005200/CBET005290.txt

Zhai, C., Ye, Q., Shao, M., et al. 2020, PASP, 132, 064502

Zubović, D., Vida, D., Gural, P., & Šegon, D. 2015, in Proc. of the Int. Meteor Conf., ed. J. L. Rault & P. Roggemans (Int. Meteor Organization), 27